Fitoterapia 179 (2024) 106261

Contents lists available at ScienceDirect

Fitoterapia

journal homepage: www.elsevier.com/locate/fitote

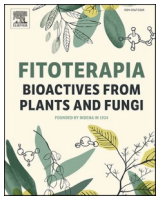

Research Paper

Hermansones A and B: Bioactive naphthazarin congeners from the European crust fungus *Hermanssonia centrifuga*

Winnie Chemutai Sum [a,b], Sherif S. Ebada [a,c,*], Jackson M. Muema [d], Harald Kellner [e], Attila Mándi [f], Tibor Kurtán [f], Marc Stadler [a,b,*]

[a] Department of Microbial Drugs, Helmholtz Centre for Infection Research GmbH (HZI) and German Centre for Infection Research, Inhoffenstrasse 7, 38124 Braunschweig, Germany
[b] Institute of Microbiology, Technische Universität Braunschweig, Spielmannstraße 7, 38106 Braunschweig, Germany
[c] Department of Pharmacognosy, Faculty of Pharmacy, Ain Shams University, 11566 Cairo, Egypt
[d] Compound Profiling and Screening (COPS), Helmholtz Centre for Infection Research (HZI), Inhoffenstraße 7, 38124 Braunschweig, Germany
[e] Department of Bio- and Environmental Sciences, Technische Universität Dresden-International Institute Zittau, Markt 23, 02763 Zittau, Germany
[f] Department of Organic Chemistry, University of Debrecen, P.O. Box 400, H-4002 Debrecen, Hungary

ARTICLE INFO

Keywords:
Naphthoquinone
Hermanssonia
Antiviral
Meruliaceae
Boryquinone

ABSTRACT

Two previously undescribed naphthazarins named hermansones A (**1**) and B (**2**), were isolated from the wood-decaying basidiomycete *Hermanssonia centrifuga*. The study presents the first report of natural products from the species. The structures of the secondary metabolites were elucidated through NMR spectroscopy and mass spectrometry. The absolute configuration of compound **1** was elucidated using TDDFT-ECD calculations. Hermansone B (**2**) demonstrated moderate inhibitory effects against Chikungunya virus at IC_{50} of 55.97 μM, without inducing notable cytotoxicity.

1. Introduction

To-date, natural sources remain unmatched reservoirs of potential drugs with health-promoting effects. In order to safeguard our future prospects for the discovery and subsequent development of potent anti-infectives, there is a dire need to delve into unexplored and/or under-explored natural niches for novel chemistry. In the recent past, various reports on the Basidiomycota has emphasized its ingenious production of valuable secondary metabolites with potential application in combating myriad ailments [1,2].

In our current study, we explored the secondary metabolome of the European red-listed wood-decaying basidiomycete *Hermanssonia centrifuga* (P. Karst.) Zmitr. (formerly *Phlebia centrifuga* P. Karst.; Meruliaceae). The genus *Phlebia* Fr. was circumscribed in 1821 by Elias Fries, a Swedish mycologist who typified it by *Phlebia radiata* Fr. and currently, around 100 species are accepted in the genus [3,4]. Despite being cosmopolitan, the genus recently demonstrated a decline in its species attributed to habitat fragmentation and reduction due to intensive deforestation, among other ecological reasons [5]. The recently coined genus *Hermanssonia*, only consists of two species until now namely *H. centrifuga* and *H. fimbriata* (https://www.indexfungorum.org/Names/Names.asp). To the best of our knowledge, no secondary metabolites have been reported from the genus thus far. Nonetheless, new isolactarane and sterpurane sesquiterpenoids possessing various antimicrobial and cytotoxic effects were reported from the related *Phlebia uda* [6]. Additionally, investigation of *P. tremellosa* afforded isolactarane and sterpurane sesquiterpenes [7,8]. On the other hand, *Puncturalia atropurpurascens*, an anamorph of the genus *Phlebia*, was reported to produce a terphenylquinone named polyporic acid, phlebiarubrone and phlebiakauranol derivatives, firstly reported from *P. strigosozonata* [9,10]. In addition, quinones with extended unbranched side chains such as phlebiachrysoric acids and the merulinic acid-derivatives ceriporiones were reported from different species of the genus *Phlebia* [11,12]. Our current investigation of *H. centrifuga* yielded two previously undescribed napthaquinones, and herein we elaborate their chemistry and biological effects.

* Corresponding authors at: Department of Microbial Drugs, Helmholtz Centre for Infection Research GmbH (HZI) and German Centre for Infection Research, Inhoffenstrasse 7, 38124 Braunschweig, Germany.
E-mail addresses: sherif.elsayed@helmholtz-hzi.de, sherif_elsayed@pharma.asu.edu.eg (S.S. Ebada), Marc.Stadler@helmholtz-hzi.de (M. Stadler).

https://doi.org/10.1016/j.fitote.2024.106261
Received 4 August 2024; Received in revised form 10 October 2024; Accepted 13 October 2024
Available online 16 October 2024

2. Materials and methods

2.1. General experimental procedures

HPLC-DAD/MS measurements were performed on the amaZon speed ETD ion trap mass spectrometer (Bruker Daltonics, Bremen, Germany) using positive and negative ionization modes, simultaneously. The HPLC system consisted of a C_{18} Acquity UPLC BEH (Waters) column as the stationary phase, and solvent A [deionized water + 0.1 % formic acid] / solvent B [acetonitrile (MeCN) + 0.1 % formic acid] as the mobile phase. The elution gradient began at 5 % B for 0.5 min, followed by a gradual increase to 100 % B in 20 min. Thereafter, an isocratic condition was maintained at 100 % B for 10 min. The system's flow rate was 0.6 mL/min and the UV/Vis detections were recorded at 210 nm and scanned over 190–600 nm spectrum. HR-ESI-MS (high-resolution electrospray ionization mass spectrometry) was acquired using the timsTOF Pro 2 mass spectrometer (Bruker Daltonics, Bremen, Germany) connected to an Agilent 1290 series HPLC-UV system (Agilent Technologies, Santa Clara, CA, USA) equipped with C_{18} Acquity UPLC BEH column (Waters, Milford, USA) as a stationary phase. The solvent system used included solvent A (deionized water + 0.1 % formic acid) and solvent B (MeCN + 0.1 % formic acid). The gradient of separation was as follows: 5 % B for 0.5 min, 100 % B over a period of 20 min, and isocratic separation at 100 % B for 5 min. The flow rate was maintained at 0.6 mL/min (40 °C) and the UV detections recorded at 210 nm. To determine the molecular formulas of the compounds, Smart Formula algorithm (Bruker Daltonics) of the Compass DataAnalysis 6.1 software was employed.

Optical rotations were recorded in methanol (Uvasol, Merck, Darmstadt, Germany) using the Anton Paar MCP-150 polarimeter (Seelze, Germany) at 20 °C. UV/Vis spectra were recorded using the Shimadzu UV/Vis 2450 spectrophotometer (Kyoto, Japan) at a concentration of 0.02 mg/mL in methanol (Uvasol). ECD spectra were measured on a J-815 spectropolarimeter (JASCO, Pfungstadt, Germany). The NMR spectra were measured on Avance III 500 (Bruker, Bremen, Germany) (^{1}H NMR: 500 MHz and ^{13}C NMR: 125 MHz) spectrometer locked to the respective deuterium signal of the solvent.

Solvents (analytical and HPLC grade) and chemicals were purchased from AppliChem GmbH (Darmstadt, Germany), Carl Roth GmbH & Co. KG (Karlsruhe, Germany), Avantor Performance Materials (Deventer, Netherlands) and Merck (Darmstadt, Germany). Deionized water was obtained from the PURELAB flex water purification system (Veolia Water Technologies, Celle, Germany).

2.2. Collection and culturing of the fungus

The fungal material was collected and identified by one of the authors (H.K.) from Bavaria, Germany. The specimen was found on a lying decomposing *Fagus sylvatica* log at Mittelsteighütte in the Bavarian Forest National Park (Germany), in October 2022. The axenic mycelial cultures were then established and maintained in YMG (yeast-malt-glucose) medium consisting of malt extract 10 g/L, yeast extract 4 g/L, D-glucose 4 g/L, agar 20 g/L, at pH 6.3), as previously described [13]. Subsequently, fully-grown mycelial cultures were used to inoculate 5 × 500 mL Erlenmeyer flasks consisting of rice media, prepared as earlier described [13]. A copy of the culture was deposited at the International Institute Zittau, Technical University of Dresden (Germany) as IHI 754 (*Hermanssonia centrifuga*).

2.3. Extraction and isolation of **1** and **2**

Following incubation (24 °C) under static conditions for 36 days, the rice cultures were extracted. In brief, the cultures were initially soaked overnight in 500 mL acetone per flask and later extracted under ultrasonic bath (40 °C) with an equal amount of acetone thrice. The solvent was then evaporated and the semi-liquid phase reconstituted in distilled water and partitioned twice with ethyl acetate (ratio 1:1). After filtration and dehydration through anhydrous sodium sulphate (Na_2SO_4), the aqueous phase was discarded and the organic phase was dried on a rotary evaporator (Heidolph Instruments GmbH & Co. KG, Schwabach, Germany; pump: Vacuubrand GmbH & Co. KG, Wertheim am Main, Germany), to yield a total extract (1.4 g). The extract was purified and the compounds were isolated using preparative reversed phase liquid chromatography system (PLC 2020; Gilson, Middleton, WI, USA). The system was equipped with a VP Nucleodur 100–5 C-18 ec packed column (250 × 40 mm, 7 µm, Macherey-Nagel, Düren, Germany) as the stationary phase. The elution phase consisted of deionized water + 0.1 % formic acid (solvent A) and MeCN + 0.1 % formic acid (solvent B). The implemented separation gradient began at 5 % B for 5 min, followed by an increase to 10 % B in 3 min. Subsequently, the gradient was run between 10–50 % B over 40 min, followed by 50–100 % in 5 min and a final holding at 100 % B for 10 min. The UV detections were made at 210 and 350 nm and the flow rate was set at 40 mL/min. The separation method led to the isolation of hermansones A (**1**) (5.7 mg, t_R = 12 min) and B (**2**) (4.0 mg, t_R = 15 min).

2.3.1. Hermansone A (2,3-Hydroisoaureoquinone) (1)

Yellow oil; $[\alpha]_D^{20}$ +10 (*c* 0.1, MeOH); UV–Vis (MeOH) λ_{max} (log ε): 201.5 (4.01), 214.5 (4.02), 270 (4.00), 322.5 (3.71), 429 (3.40); ECD (0.93 mM, MeOH) λ_{max} ($\Delta\varepsilon$): 343 (−5.09), 309 (+3.02), 272sh (+0.77), 246 (−1.38), 228 (+0.07), 208 (−3.79); NMR data (^{1}H: 500 MHz, ^{13}C: 125 MHz, methanol-d_4, DMSO-d_6) see Table 1; HR-ESI-MS: *m/z* 251.0551 $[M - H_2O + H]^+$ (calcd. 251.0550 for $C_{12}H_{11}O_6^+$), 269.0656 $[M + H]^+$ (calcd. 269.0656 for $C_{12}H_{13}O_7^+$), 291.0476 $[M + Na]^+$ (calcd. 291.0475 for $C_{12}H_{12}NaO_7^+$), t_R = 2.20 min (LR-ESI-MS); $C_{12}H_{12}O_7$ (268.01 g mol^{-1}).

2.3.2. Hermansone B (Isoaureoquinone) (2)

Orange oil; UV–Vis (MeOH) λ_{max} (log ε): 201.5 (4.03), 268.5 (4.22), 332 (3.78); NMR data (^{1}H: 500 MHz, ^{13}C: 125 MHz, methanol-d_4, DMSO-d_6) see Table 1; HR-ESI-MS: *m/z* 251.0553 $[M + H]^+$ (calcd. 251.0550 for $C_{12}H_{11}O_6^+$); t_R = 6.07 min (LR-ESI-MS); $C_{12}H_{10}O_6$ (250.01 g mol^{-1}).

2.4. Cytotoxicity assay.

The most sensitive mammalian cell lines namely human endocervical adenocarcinoma (KB3.1) and mouse fibroblasts (L929), were sourced from the German Collection of Microorganisms and Cell Cultures (DSMZ, Braunschweig, Germany) and used in the determination of the half-maximal inhibitory concentration (IC_{50}) of compounds **1** and **2**. The assay was performed using the MTT (3-(4,5-dimethylthiazol-2-yl)-2,5-diphenyltetrazolium bromide) in 96-well microtiter plates in accordance with our standard protocol [14]. Epothilone B and methanol were used as positive and negative controls, respectively.

Table 1
1D (^{1}H and ^{13}C) NMR data of **1** and **2**.

	1				2			
pos.	δ_C,[a] type	δ_H[a] multi (*J*[Hz])	δ_C,[b] type	δ_H[b] multi (*J*[Hz])	δ_C,[a] type	δ_H[a] multi (*J*[Hz])	δ_C,[b] type	δ_H[b] multi (*J*[Hz])
1	200.5, CO		198.6, CO		188.3, CO		186.0, CO	
2	81.5, C		78.7, C		122.5, C		120.7, C	
3	79.6, CH	4.49 s	78.7, CH	4.17 s	154.9, C		153.7, C	
4	201.7, CO		201.9, CO		185.5, CO		183.6, CO	
4a	111.6, C		110.1, C		108.9, C		107.1, C	
5	150.2, C		149.1, C		151.6, C		150.2, C	
6	138.1, C		136.2, C		137.1, C		135.7, C	
7	152.6, C		151.1, C		152.4, C		150.2, C	
8	123.3, C		120.5, C		126.1, C		124.2, C	
8a	124.5, C		123.9, C		123.0, C		121.3, C	
9	20.0, CH_3	1.26 s	20.0, CH_3	1.21 s	8.9, CH_3	1.95 s	9.0, CH_3	1.86 s
10	12.7, CH_3	2.45 s	12.4, CH_3	2.32 s	13.3, CH_3	2.50 s	13.1, CH_3	2.42 s

[a] Measured in methanol-d_4 at 125 MHz for ^{13}C and 500 MHz for ^{1}H.
[b] Measured in DMSO-d_6 at 125 MHz for ^{13}C and 500 MHz for ^{1}H.

2.5. Antimicrobial assay

Minimum inhibitory concentrations (MICs) of the compounds were determined via serial dilutions on 96-well microtiter plates against various test microorganisms in accordance with our established protocol [14]. Clinically relevant fungal and bacterial test pathogens comprised *Bacillus subtilis* (DSM 10), *Staphylococcus aureus* (DSM 346), *Acinetobacter baumannii* (DSM 30008), *Escherichia coli* (DSM 1116), *Chromobacterium violaceum* (DSM 30191), *Pseudomonas aeruginosa* (PA14), *Candida albicans* (DSM 1665), *Mycobacterium smegmatis* (ATCC 700084), *Mucor hiemalis* (DSM 2656), *Schizosaccharomyces pombe* (DSM 70572), *Rhodotorula glutinis* (DSM 10134) and *Pichia anomala* (DSM 6766), obtained from the DSMZ (Braunschweig, Germany). Nystatin was used as the positive control against fungi, whereas ciprofloxacin, gentamicin, kanamycin and oxytetracycline were employed as standard drugs against bacteria.

2.6. Antiviral activity testing

Antiviral activity was evaluated against Chikungunya virus (CHIKV^{Gluc})-infected Huh7.5.1 cells at a multiplicity of infection (MOI) of 0.01. Briefly, 2×10^4 cells/well were seeded in a 96-well plate and allowed for 24 h to adhere. The spent medium was aspirated off and replaced with 50-μL virus suspension and 50-μL of compound dilutions (2-fold diluted from a maximal concentration of 50 μM in Dulbecco's Modified Eagle Medium (DMEM)). Then, an aliquot of 0.5 % DMSO and ribavirin served as negative and positive controls, respectively. The plate was incubated for 72 h under standard culture conditions of 37 °C and 5 % CO_2. Viral infection intensity following compound treatment was quantified by aliquoting 8-μL of supernatants into a new 96-well plate, mixing with 10-μL Renilla luciferase reagent, and luminescence read using a Synergy H1 microplate reader. In parallel, cytotoxicity effects were performed on a separate batch of cells by CellTiter®-Glo assay (Promega, Cat. #G9241) as per manufacturer's instructions. Two independent experimental replicates were performed ($n = 2$).

2.7. Computational section

Mixed torsional/low-mode conformational searches were carried out by means of the Macromodel 10.8.011 software using the Merck molecular force field (MMFF) with an implicit solvent model for $CHCl_3$ applying a 21 kJ/mol energy window [15]. Geometry re-optimizations of the resultant conformers (ωB97X/TZVP PCM/MeOH, SOGGA11-X/TZVP SMD/MeOH) and TDDFT-ECD calculations were performed with Gaussian 16 using various functionals (B3LYP, BH&HLYP, CAMB3LYP, PBE0) and the TZVP basis set with the same solvent model as in the preceding DFT optimization step [16]. ECD spectra were generated as the sum of Gaussians with 2400 and 3000 cm^{-1} half-height width, using dipole velocity-computed rotational strength values [17]. Boltzmann distributions were estimated from the ωB97X and SOGGA11-X energies. The MOLEKEL program was used for visualization of the results [18].

3. Results and discussion

3.1. Structure elucidation of compounds *1* and *2*.

Compound **1** was isolated as a yellow oil. Its molecular formula was established as $C_{12}H_{12}O_7$ indicating seven degrees of unsaturation based on its HR-ESI-MS that revealed a protonated molecular ion and a sodium adduct at *m/z* 269.0656 $[M + H]^+$ (calculated 269.0656) and 291.0476 $[M + Na]^+$ (calculated 291.0475), respectively. The ^{1}H NMR spectral data of **1** (Table 1, Fig. S3) revealed three singlet signals, one singlet proton (δ_H 4.49) and two methyl groups distinguished into one olefinic (δ_H 2.45) and one aliphatic (δ_H 1.26). The ^{13}C NMR and HSQC spectral data of **1** (Table 1, Figs. S4, S7) revealed twelve different carbon resonances including nine unprotonated carbons categorized into two carbonyl carbon atoms (δ_C 201.7, 200.5), three oxygenated sp^2 carbon atoms (δ_C 152.6, 150.2, 138.1), three sp^2 carbon (δ_C 124.5, 123.3, 111.6) and one sp^3 carbon (δ_C 81.5). In addition, the ^{13}C NMR and HSQC spectra confirmed the presence of one methine sp^3 carbon (δ_C 79.6) and two sp^3 carbon atoms (δ_C 20.0, 12.7). A literature search of **1** based on the obtained results suggested it to be a naphthazarin derivative related to aureoquinone, a potent protease inhibitor from *Aureobasidium* sp. and talcarpones, antifungal bisnaphthazarin derivatives from *Talaromyces johnpittii* [19,20]. The ^{1}H—^{1}H COSY spectrum of **1** (Figs. 2, S5) revealed a long-range cross peak between a proton signal at δ_H 4.49 and a methyl peak at δ_H 1.26 ppm assigned to H-3 and H_3–9, respectively. Further confirmation to the depicted structure of **1** was obtained via its HMBC spectrum (Figs. 2, S6) that revealed key correlations from olefinic

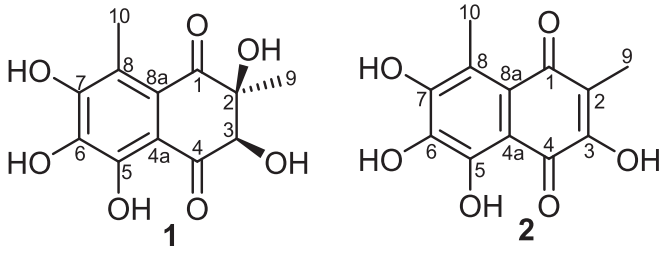

Fig. 1. Chemical structures of **1** and **2**.

methyl group H_3–10 to four carbon atoms at δ_C 200.5 (C-1), 111.6 (C-4a), 152.6 (C-7), 123.3 (C-8) and 124.5 (C-8a) indicating its binding at C-8. The HMBC spectrum of **1** (Fig. 2) also revealed correlations from an aliphatic methyl group H_3–9 to C-1, C-2 (δ_C 81.5) and C-3 (δ_C 79.6) confirming its position at C-2.

The relative configuration of **1** was determined by the ROESY spectrum (Figs. 2, S10) that revealed key correlations from H_3–9 to H-3 at δ_H 4.49 (s) supporting their projection toward the same face of the molecule. Accordingly, the (2*S**,3*R**) relative configuration of **1** was assigned. In order to determine the absolute configuration, the TDDFT-ECD protocol was applied on the arbitrarily chosen (2*S*,3*R*) stereoisomer of **1**. The Merck molecular force field (MMFF) conformational search of (2*S*,3*R*)-**1** resulted in 5 conformers within a 21 kJ/mol energy window, which were re-optimized at the ωB97X/TZVP [21] PCM/MeOH level. Boltzmann-averaged ECD spectra computed for these conformers gave weak to moderate agreement with the experimental ECD spectrum at four different levels of theory (see Fig. S11). Although the ωB97X functional was identified as one of the best-performing in terms of energy and geometrical parameters according to a recent benchmark study [22] and we also had several examples where the ωB97X performed well [23], all functionals are approximations and thus have a certain amount of possible error [24], and there is no single supreme functional that would work well in all cases. To improve the agreement, another well-performing functional, the SOGGA11-X [25], was tested with TZVP basis set and the SMD solvent model MeOH for the re-optimization of the MMFF conformers. Boltzmann-averaged ECD spectra computed for these conformers gave a good agreement with the experimental ECD spectrum at various levels, underestimating only the positive shoulder at 272 nm (Fig. 3). By comparing the low-energy conformers obtained at the ωB97X and the SOGGA11-X levels, it is evident that the SOGGA11-X estimated conformer B (and the *P* helicity conformers in general) similarly populated as conformer A (Fig. S12), while with the ωB97X functional, conformer A (and the *M* helicity conformers in general) was 3.5 times more populated than conformer B (Fig. S13). In conformer A, the C-2 methyl group adopted *equatorial* orientation with *M* helicity of the condensed carbocyclic ring, while in conformer B, the condensed ring flipped to the *P* helicity form shifting the C-2 methyl group to the *axial* position. The computed ECD curves of the *P* helicity conformers (Fig. 4) provided a good agreement with the experimental ECD, while the *M* helicity ones showed a mismatch. It is known from the literature that a wrong estimation of the Boltzmann distribution can lead to a misassignment in some cases [26], and there are also literature examples where not the lowest-energy but a less-populated conformer or conformer group governs the ECD spectrum [27]. The small absolute value of the specific rotation did not enable the unambiguous application of optical rotation (OR) calculation for determiningthe absolute configuration. On the basis of ECD calculation results, the absolute configuration of **1** was elucidated as (2*S*,3*R*). In conclusion, compound **1** was identified as a previously undescribed (2*S*,3*R*)-hydroisoaureoquinone derivative that was trivially named hermansone A.

Compound **2** is isolated as an orange oil with its molecular formula determined to be $C_{12}H_{10}O_6$ indicating eight degrees of unsaturation based on the HR-ESI-MS revealing a protonated molecular ion peak at *m/z* 251.0553 $[M + H]^+$ (calculated 251.0550). By comparing the molecular formulas of **1** and **2**, they revealed that **2** is a dehydrated derivative of **1**. The ^{1}H NMR spectral data of **2** (Table 1, Fig. S16) simply revealed the presence of two olefinic methyl groups at δ_H 2.50 (H_3−10) and 1.95 (H_3–9) while its ^{13}C NMR spectral data (Table 1, Fig. S17) revealed twelve carbon resonances categorized by the HSQC spectrum (Fig. S20) into two carbonyl carbon atoms (δ_C 188.3, 185.5), four oxygenated olefinic carbon atoms (δ_C 154.9, 152.4, 151.6, 137.1), four unprotonated olefinic carbon atoms (δ_C 126.1, 123.0, 122.5, 108.9). A literature search of **2** suggested its structural similarity to aureoquinone [19,20].

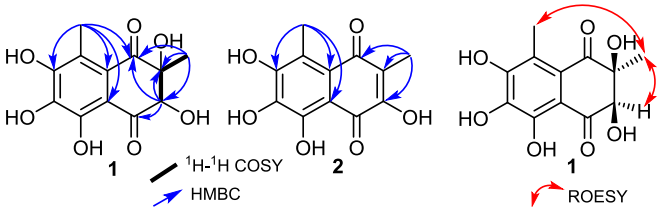

Fig. 2. Key ^{1}H—^{1}H COSY, HMBC and ROESY correlations of **1** and **2**.

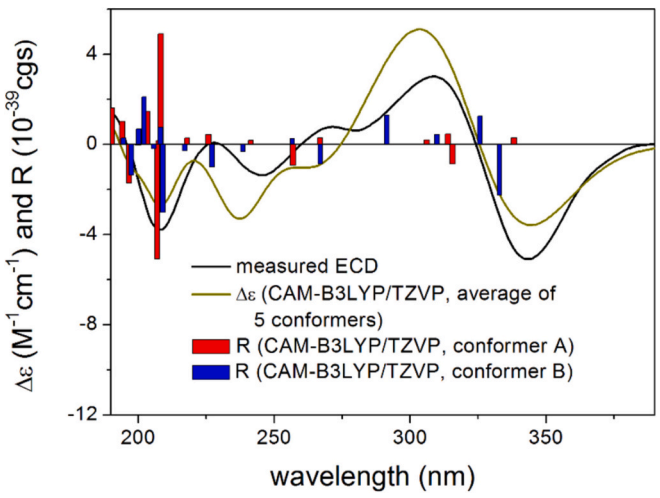

Fig. 3. Experimental ECD spectrum of **1** (black) compared with the CAM-B3LYP/TZVP SMD/MeOH ECD spectrum of (2*S*,3*R*)-**1** (olive). Level of DFT optimization: SOGGA11-X/TZVP SMD/MeOH. Bars represent the computed rotational strength values of conformers A (red) and B (blue). (For interpretation of the references to colour in this figure legend, the reader is referred to the web version of this article.)

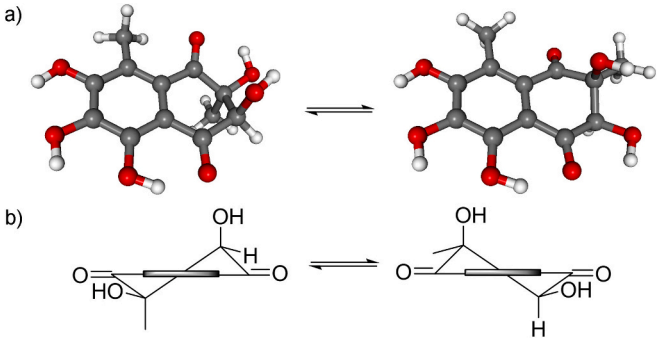

Fig. 4. Conformational equilibrium of the *M* (left) and *P* (right) helicity conformers of (2*S*,3*R*)-**1**. a) Lowest-energy *M*- and *P*-helicity conformers (conformers A and B, respectively, at the SOGGA11-X/TZVP SMD/MeOH level). b) Projective formulas indicating the ring helicity. Estimated sum Boltzmann distributions of the two forms (*M* vs. *P*) were 73.0 % vs. 27.0 % at the ωB97X/TZVP PCM/MeOH level and 44.5 % vs. 55.5 % at the SOGGA11-X/TZVP SMD/MeOH level. The thick line represents the condensed benzene ring.

A comparison of ^{13}C NMR data of **2** (Table 1) and aureoquinone [19,20] revealed obvious differences in the carbon resonances assinged for C-5 to C-8 suggesting an alternative substitution pattern. Further confirmation to the depicted structure of **2** (Fig. 1) was provided by the HMBC spectrum (Figs. 2, S19) that revealed key correlations from H_3–10 to four carbon atoms at δ_C 188.3 (C-1), 108.9 (C-4a), 152.4 (C-7), 126.1 (C-8) and 123.0 (C-8a) indicating its binding at C-8. The second olefinic methyl group at δ_H 1.95 (H_3–9; δ_C 8.9) revealed key HMBC correlations to C-1, C-2 (δ_C 122.5) and C-3 (δ_C 154.9) confirming its position at C-2. Based on the obtained results, compound **2** was confirmed to be a

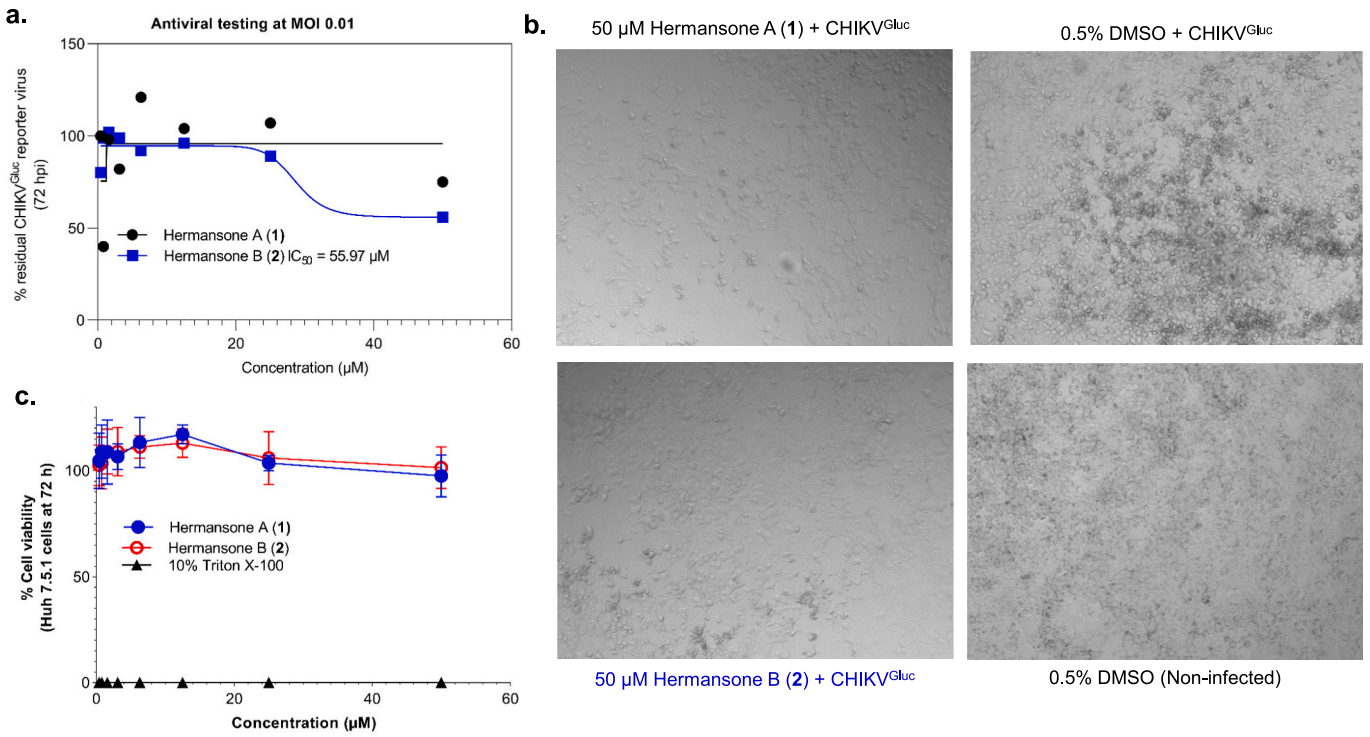

Fig. 5. Antiviral activity of **1** and **2** against Chikungunya (CHIKV^{Gluc}) virus. **a**. Dose-response curve for the anti-CHIKV activity afforded by compounds **1** and **2** at 72-hpi. Each plotted dot is a mean value of two independent experimental replicates ($n = 2$). The dose-response curve was generated using a non-linear regression algorithm on Graphpad Prism (v. 9.3.1) software. **b**. Bright field microscopic images from treated wells alongside infected [+ 0.5 % dimethylsulfoxide (DMSO)] and non-infected (+ 0.5 % DMSO) references. Images were taken on the same date of activity read-out using EVOS™ M5000 Imaging System. **c**. Cell viability assay of **1** and **2** on Huh 7.5.1 cells using CellTiter®-Glo (Promega). A 10 % Triton X-100 served as a positive control. Data presented as a mean ± standard deviation (SD) of two independent replicates and six technical replicates.

previously undescribed structural isomer of aureoquinone that was named hermansone B.

3.2. Biological evaluation

The two isolated compounds **1** and **2** revealed no antimicrobial effect. Additionally, they were non-cytotoxic against KB3.1 and L929 cell lines, considered as the most sensitive cell lines in the assay. Hence, further assessment against other cell lines were not considered. Antiviral testing of the isolated compounds indicated potential structural-based activity differences. Relative to ribavirin that achieved 95 % anti-CHIKV activity at the tested concentration (50 µM; Fig. S23), the compounds; hermansones A and B, achieved a 40–47 % anti-infectivity effect at the same concentration (Fig. 5a). While both hermansones A and B at 50 µM exerted nearly equal antiviral activity (Fig. 5a-b), hermansone A depicted a generally unstable effect. Hermansone B showed a considerably moderate anti-CHIKV activity with an average IC_{50} value of 55.97 ± 0.27 µM. All the compounds had no obvious cytotoxic effects on Huh 7.5.1 cells (Fig. 5c), suggesting a broad selective window for the antiviral effect of hermansone B (**2**).

4. Conclusions

The exploration of solid-state rice cultures of the white-rot fungus *Hermanssonia centrifuga* (P. Karst.) Zmitr. afforded two previously undescribed napthaquinones **1** and **2**, whereby hermansone B (**2**) had moderate antiviral effect against Chikungunya virus without overt cytotoxicity. Hermansone B (2) featured an α,β-unsaturated carbonyl moiety, compared to its inactive congener, hermansone A (**1**), acting as a Michael acceptor, previously reported to be associated with antiviral effects [28] and other diverse medicinal properties [29]. This explains in part the revealed antiviral effect of **2** compared to **1**. Nonetheless, further research on napthaquinone analogs remain worthwhile in order to conclusively deduce their structure activity relationships.

CRediT authorship contribution statement

Winnie Chemutai Sum: Conceptualization, Isolation, Analysis of compounds, original manuscript writing. **Sherif S. Ebada:** Writing – review & editing, Writing – original draft, Supervision, Data curation, Conceptualization. **Jackson M. Muema:** Methodology. **Harald Kellner:** Resources. **Attila Mándi:** Validation, Software. **Tibor Kurtán:** Writing – review & editing, Methodology. **Marc Stadler:** Writing – review & editing, Supervision, Conceptualization.

Declaration of competing interest

The authors declare the following financial interests/personal relationships which may be considered as potential competing interests: Sherif S. Ebada reports financial support was provided by Alexander von Humboldt Foundation. Winnie C. Sum reports financial support was provided by German Academic Exchange Service. Tibor Kurtan reports financial support was provided by National Research Development and Innovation Office. Jackson M. Muema reports financial support was provided by Alexander von Humboldt Foundation. Marc Stadler is a member of the Editorial Board of Fitoterapia. If there are other authors, they declare that they have no known competing financial interests or personal relationships that could have appeared to influence the work reported in this paper.

Acknowledgements

W.C.S. is grateful to the German Academic Exchange Service (DAAD) for the doctoral scholarship funding (Program number 57507871). S.S.E. gratefully acknowledges the Alexander von Humboldt (AvH) Foundation for granting him the Georg-Forster Fellowship for Experienced Researchers Stipend (Ref 3.4-1222288-EGY-GF-E). J.M.M. appreciates the support of the Alexander von Humboldt (AvH) Bayer Science Foundation on Humboldt Research Fellowship for Postdoctoral Researchers. The authors are grateful to Myriam Friemelt and Ursula Bilitewski for their facilitation with the antiviral assay. T.K. and A.M. were supported by the National Research Development and Innovation Office (K138672 and FK134653). The Governmental Information-Technology Development Agency (KIFÜ) is acknowledged for CPU time. We thank the Bavarian Forest National Park and the Mycology group of the Department of Conservation and Research for support and sample permissions.

Appendix A. Supplementary data

Supplementary data to this article can be found online at https://doi.org/10.1016/j.fitote.2024.106261.

Data availability

All data are included in the main text and its supplementary material file.

References

[1] M. Gressler, N.A. Löhr, T. Schäfer, S. Lawrinowitz, P.S. Seibold, D. Hoffmeister, Mind the mushroom: natural product biosynthetic genes and enzymes of Basidiomycota, Nat. Prod. Rep. 38 (2021) 702–722, https://doi.org/10.1039/D0NP00077A.

[2] W.C. Sum, S.S. Ebada, J.C. Matasyoh, M. Stadler, Recent progress in the evaluation of secondary metabolites from Basidiomycota, Curr. Res. Biotechnol. 6 (2023) 100155, https://doi.org/10.1016/j.crbiot.2023.100155.

[3] N.N. Wijayawardene, K.D. Hyde, D.Q. Dai, M. Sánchez-García, B.T. Goto, R. K. Saxena, M. Erdoğdu, F. Selçuk, K.C. Rajeshkumar, et al., Outline of Fungi and fungus-like taxa–2021, Mycosphere 13 (2022) 53–453, https://doi.org/10.5943/mycosphere/13/1/2.

[4] C. Zhao, M. Qu, R. Huang, S.C. Karunarathna, Multi-gene phylogeny and taxonomy of the wood-rotting fungal genus *Phlebia sensu lato* (Polyporales, Basidiomycota), J. Fungi 9 (2023) 320, https://doi.org/10.3390/jof9030320.

[5] I.N.A. Franzén, R. Vasaitis, R. Penttilä, J.A.N. Stenlid, Population genetics of the wood-decay fungus *Phlebia centrifuga* P. Karst. In fragmented and continuous habitats, Mol. Ecol. 16 (2007) 3326–3333, https://doi.org/10.1111/j.1365-294X.2007.03394.x.

[6] A. Schüffler, B. Wollinsky, T. Anke, J.C. Liermann, T. Opatz, Isolactarane and sterpurane sesquiterpenoids from the basidiomycete *Phlebia uda*, J. Nat. Prod. 75 (2012) 1405–1408, https://doi.org/10.1021/np3000552.

[7] W.C. Sum, N. Mitschke, H. Schrey, K. Wittstein, H. Kellner, M. Stadler, J. C. Matasyoh, Antimicrobial and cytotoxic cyathane-xylosides from cultures of the basidiomycete *Dentipellis fragilis*, Antibiotics 11 (2022) 1072, https://doi.org/10.3390/antibiotics11081072.

[8] W. Quack, T. Anke, F. Oberwinkler, B.M. Giannetti, W. Steglich, Antibiotics from Basidiomycetes. V Merulidial, a new antibiotic from the basidiomycete *Merulius tremellosus* Fr, J. Antibiot. 31 (8) (1978) 737–741, https://doi.org/10.7164/antibiotics.31.737.

[9] M. Jonassohn, H. Anke, O. Sterner, C. Svensson, New compounds isolated from the culture filtrate of the fungus *Merulius tremellosus*, Tetrahedron Lett. 35 (10) (1994) 1593–1596, https://doi.org/10.1016/S0040-4039(00)76767-0.

[10] H., Anke, I., Casser, R., Herrfnann, W. Steglich, New terphenylquinones from mycelial cultures of *Punctularia atropurpurascens* (Basidiomycetes), Z. Naturforsch. C 39 (7–8) (1984) 695–698, https://doi.org/10.1515/znc-1984-7-801.

[11] M., Gill, W., Steglich, Pigments of fungi (Macromycetes), in: W. Herz, H. Grisebach, G.W. Kirby, C. Tamm (Eds.), Progress in the Chemistry of Organic Natural Products vol. 51, Springer Verlag, Wien, New York, 1987, pp. 1–317, https://doi.org/10.1007/978-3-7091-6971-1_1.

[12] M., Gill, Pigments of fungi (Macromycetes), Nat. Prod. Rep. 16 (1999) 301–317, https://doi.org/10.1039/A705730J.

[13] H. Anke, I. Casser, W. Steglich, E.H. Pommer, Antibiotics from basidiomycetes. 26 Phlebiakauranol aldehyde an antifungal and cytotoxic metabolite from *Punctularia atropurpurascens*, J. Antibiot. 40 (4) (1987) 443–449, https://doi.org/10.7164/antibiotics.40.443.

[14] P., Pripdeevech, S., Khruengsai, C., Tanapichatsakul, W.M., Afifi, W.C., Sum, K.D., Hyde, S.S. Ebada, Cytotoxic polyhydroxy-isoprenoids from *Neodidymelliopsis negundinis*, J. Nat. Prod. 87 (2024) 349–357, https://doi.org/10.1021/acs.jnatprod.3c01094.

[15] MacroModel, Schrödinger LLC. https://newsite.schrodinger.com/platform/products/macromodel/, 2015.

[16] M.J. Frisch, G.W. Trucks, H.B. Schlegel, G.E. Scuseria, M.A. Robb, J.R. Cheeseman, G. Scalmani, V. Barone, G.A. Petersson, H. Nakatsuji, et al., Gaussian 16, Revision C.02, Gaussian, Inc, Wallingford CT, USA, 2019.

[17] P.J. Stephens, N. Harada, ECD cotton effect approximated by the Gaussian curve and other methods, Chirality 22 (2010) 229–233, https://doi.org/10.1002/chir.20733.

[18] U. Varetto, MOLEKEL 5.4, Swiss National Supercomputing Centre, Manno, Switzerland, 2009.

[19] A. Berg, H. Görls, H. Dörfelt, G. Walther, B. Schlegel, U. Gräfe, Aureoquinone, a new protease inhibitor from *Aureobasidium* sp. J. Antibiot. 53 (2000) 1293–1295, https://doi.org/10.7164/antibiotics.53.1293.

[20] A.E. Lacey, S.A. Minns, R. Chen, D. Vuong, E. Lacey, J.A. Kalaitzis, Y.P. Tan, R. G. Shivas, M.S. Butler, A.M. Piggott, Talcarpones A and B: bisnaphthazarin-derived metabolites from the Australian fungus *Talaromyces johnpittii* sp. nov. MST-FP2594, J. Antibiot. 77 (2024) 147–155, https://doi.org/10.1038/s41429-023-00688-x.

[21] J.D. Chai, M. Head-Gordon, Long-range corrected hybrid density functionals with damped atom–atom dispersion corrections, Phys. Chem. Chem. Phys. 10 (2008) 6615–6620, https://doi.org/10.1039/B810189B.

[22] É. Brémond, M. Savarese, N.Q. Su, Á.J. Pérez-Jiménez, X. Xu, J.C. Sancho-García, C. Adamo, Benchmarking density functionals on structural parameters of small−/medium-sized organic molecules, J. Chem. Theory Comput. 12 (2016) 459–465, https://doi.org/10.1021/acs.jctc.5b01144.

[23] a)A. Sikandar, A. Popoff, R.P. Jumde, A. Mándi, A. Kaur, W.A.M. Elgaher, L. Rosenberger, S. Hüttel, R. Jansen, M. Hunter, J. Köhnke, A.K.H. Hirsch, T. Kurtán, R. Müller. Revision of the absolute configurations of chelocardin and amidochelocardin. Angew. Chem. Int. Ed. 62 (2023) e202306437; doi: https://doi.org/10.1002/anie.202306437 b) S.Z. Huang, Q. Wang, J.Z. Yuan, C.H. Cai, H. Wang, A. Mándi, T. Kurtán, H.F. Dai, Y.X. Zhao. Hexahydroazulene-2(1*H*)-one sesquiterpenoids with bridged cyclobutane, oxetane, and tetrahydrofuran rings from the stems of *Daphne papyracea* with α-glycosidase inhibitory activity. J. Nat. Prod. 85 (2022) 3–14; doi: https://doi.org/10.1021/acs.jnatprod.0c01394 c) H.L. Wang, R. Li, J. Li, J. He, Z.Y. Cao, T. Kurtán, A. Mándi, G.L. Zheng, W. Zhang. Alternarin A, a drimane meroterpenoid, suppresses neuronal excitability from the coral-associated fungi *Alternaria* sp. ZH-15. Org. Lett. 22 (2020) 2995–2998; doi: https://doi.org/10.1021/acs.orglett.0c00746.

[24] a)W.N. Setzer. Conformational analysis of thioether musks using density functional theory. Int. J. Mol. Sci. 10 (2009) 3488–3501; doi: https://doi.org/10.3390/ijms10083488 b) R. Christensen, H.A. Hansen, T. Vegge. Identifying systematic DFT errors in catalytic reactions. Catal. Sci. Technol. 5 (2015) 4946; doi: https://doi.org/10.1039/C5CY01332A c) G. Pescitelli, T. Bruhn. Good computational practice in the assignment of absolute configurations by TDDFT calculations of ECD spectra. Chirality 28 (2016) 466–474; doi: https://doi.org/10.1002/chir.22600.

[25] a) R. Peverati and D. G. Truhlar. Communication: A global hybrid generalized gradient approximation to the exchange-correlation functional that satisfies the second-order density-gradient constraint and has broad applicability in chemistry. J. Chem. Phys. 135 (2011a) 191102; doi: https://doi.org/10.1063/1.3663871 b) A. Mándi, J. Wu, T. Kurtán. TDDFT-ECD and DFT-NMR studies of thaigranatins A–E and granatumin L isolated from *Xylocarpus granatum*. RSC Adv. 10 (2020) 32216; doi: https://doi.org/10.1039/D0RA03725G.

[26] a) P. Sun, D.X. Xu, A. Mándi, T. Kurtán, T.J. Li, B. Schulz, W. Zhang. Structure, absolute configuration, and conformational study of 12-membered macrolides from the fungus *Dendrodochium* sp. associated with the sea cucumber *Holothuria nobilis* Selenka. J. Organomet. Chem. 78 (2013a) 7030–7047; doi: https://doi.org/10.1021/jo400861j b) S. Superchi, P. Scafato, M. Górecki, G. Pescitelli. Configuration determination by quantum mechanical calculation of chiroptical Spectra: Basics and applications to fungal metabolites. Curr. Med. Chem. 25 (2018) 287–320; doi: https://doi.org/10.2174/0929867324666170310112009.

[27] A. Mándi, I.W. Mudianta, T. Kurtán, M.J. Garson, Absolute configuration and conformational study of psammaplysins A and B from the Balinese marine sponge *Aplysinella strongylata*, J. Nat. Prod. 78 (2015) 2051–2056, https://doi.org/10.1021/acs.jnatprod.5b00369.

[28] H.I. El-Subbagh, S.M. Abu-Zaid, M.A. Mahran, F.A. Badria, A.M. Al-Obaid, Synthesis and biological evaluation of certain α,β-unsaturated ketones and their corresponding fused pyridines as antiviral and cytotoxic agents, J. Med. Chem. 43 (2000) 2915–2921, https://doi.org/10.1021/jm000038m.

[29] M. Hossain, U. Das, J.R. Dimmock, Recent advances in α,β-unsaturated carbonyl compounds as mitochondrial toxins, Eur. J. Med. Chem. 183 (2019) 111687, https://doi.org/10.1016/j.ejmech.2019.111687.